Nanoporous Graphene as a Desalination Membrane: A Computational Study

ARCHIVES
MASSACHUSETTS INSTITUTE OF TECHNOLOGY
JUL 06 2012
LIBRARIES

by

David H. Cohen-Tanugi

Submitted to the Department of Materials Science and Engineering
in partial fulfillment of the requirements for the degree of

Masters of Science in Materials Science and Engineering

at the

MASSACHUSETTS INSTITUTE OF TECHNOLOGY

June 2012

© Massachusetts Institute of Technology 2012. All rights reserved.

Author .....
Department of Materials Science and Engineering
May 9, 2012

Certified by .....
Professor Jeffrey C. Grossman
Carl Richard Soderberg Professor Associate Professor of Power Engineering
Thesis Supervisor

Accepted by .....
Professor Gerbrand Ceder
Chairman, Department Committee on Graduate Theses

Nanoporous Graphene as a Desalination Membrane: A Computational Study

by

David H. Cohen-Tanugi

Submitted to the Department of Materials Science and Engineering
on May 9, 2012, in partial fulfillment of the
requirements for the degree of
Masters of Science in Materials Science and Engineering

Abstract

With conventional water sources in short and decreasing availability, new technologies for water supply have a crucial role to play in addressing the world's clean water needs in the 21st century. In this thesis, we examine how nanometer-scale pores in single-layer freestanding graphene can effectively filter NaCl salt from water. Using classical molecular dynamics, we report the desalination performance of such membranes as a function of pore size, chemical functionalization, and applied pressure. Our results indicate that the membrane's ability to prevent the salt passage depends critically on pore diameter, with pores in the 0.7-0.9 nm range allowing for water flow while blocking ions. Further, an investigation into the role of chemical functional groups bonded to the edges of graphene pores suggests that commonly occurring hydroxyl groups can roughly double the water flux thanks to their hydrophilic character. The increase in water flux comes at the expense of less consistent salt rejection performance, which we attribute to the ability of hydroxyl functional groups to substitute for water molecules in the hydration shell of the ions. Overall, our results indicate that the water permeability of this material is several orders of magnitude higher than conventional reverse osmosis membranes, and that nanoporous graphene may have a valuable role to play for water purification.

Thesis Supervisor: Professor Jeffrey C. Grossman
Title: Carl Richard Soderberg Professor Associate Professor of Power Engineering

Acknowledgments

I am thankful to Professor Jeffrey C. Grossman for his invaluable guidance, as well as to Joo-Hyoung Lee, Ateeque Malani and Alexie Kolpak for useful discussions. My research was funded by the MIT Energy Initiative and the John S. Hennessey Fellowship. Some of my calculations were performed using NERSC computing resources.

Contents

1 Introduction

Clean water is essential for virtually all other sectors of society, from drinking to agriculture and from energy supply to industrial manufacturing. Its short supply, unpredictable variability throughout the year, and uneven distribution across geographical areas makes it a critical resource in many parts of the world. Although water scarcity was long thought to be a problem of the developing countries, more relevant to Somalia than to Santa Barbara, it is rapidly resurfacing as a defining issue in the industrialized world as well [1]. And while a third of the world population continues to live without access to potable water, wealthier countries in America and Europe have already taken notice of the tremendous challenge of balancing sustained economic growth and rising energy demand with a fixed supply of water. Even in the United States, depleting reservoirs and global shifts in precipitation patterns due to climate change will only exacerbate the problem in coming decades.

With conventional water sources in short – and decreasing – availability, new technologies for water supply have a crucial role to play in addressing the world's clean water needs in the 21st century. The hydrological cycle of evaporation, precipitation, and river flow only provides a finite amount of fresh water, and many cities are tapping groundwater reservoirs faster than they can be replenished. Meanwhile, sustained population growth and increasing living standards enabled by economic growth are hitting up against the fundamental limits for water consumption required for power generation, food production and other essential sectors of economic activity.

Desalination is in many regards the most promising approach to long-term water supply. Other processes for obtaining additional fresh water certainly do exist: the treatment of municipal wastewater, which relies on chlorine-based decontamination and aerobic digestion, continues to provide a convenient option for water production. But the stock of salt water in oceans, which comprises 96.5 percent of the world's water, gives desalination the advantage of a virtually unlimited supply. The supply of seawater is also constant and predictable, thus offering a considerable benefit when droughts, floods, river diversion from neighboring countries, aquifer contamination and other risks threaten to cripple a society's livelihood at any moment [2]. Moreover, 2.4 billion people live in coastal areas, making the transport of water to population centers a comparatively economical task [3]. These advantages have driven policymakers in

many countries to give desalination of seawater a prominent position in the future water supply mix.

A major drawback of desalination is a high-energy footprint across all existing commercial techniques. Reverse osmosis, in which saltwater is sieved across a semipermeable membrane under high hydraulic pressure, is the most energy-efficient desalination technique to date, with a record of 1.8 kWh/m3 recently achieved in a commercial plant (compared with an average ~5 kWh/m3 in the 1990s) [4]. Meanwhile, thermal desalination methods such as Multi-Stage Flash and Multiple-Effect Distillation, which rely on evaporation instead of mechanical pressure to separate salt ions from pure water, are several times more energy-intensive than RO. Moreover, existing approaches cannot function without a massive infrastructure and correspondingly high capital costs.

The large energy footprint of RO desalination arises primarily from the high pumping pressures required to flow water across membranes. Although vast improvements in the engineering design of plants and in pressure exchange technology has helped to bring down the energy consumption of RO, the performance of the materials involved in the actual membranes remain the most crucial bottleneck in the search for more efficient and affordable water desalination.

2 Molecular-scale material science for desalination membranes: the state of the field

2.1 The limitations of classical RO membranes

Existing desalination technology leaves vast room for scientific advances, especially from the vantage point of materials for RO membranes. Classical RO membranes, which generally consist of an amorphous polymer active layer reinforced by a thicker support layer, are no longer the most promising framework for future advances. Even the active principle behind salt separation in polyamide active layers, a leading RO membrane design, remains poorly understood. What is known is that water flux occurs via a solution-diffusion mechanism, and that the presence of charged compounds along the membrane surface almost certainly plays a role in rejecting ions based on the Donnan exclusion principle [5]. Spectroscopy experiments have also shown that the hydrogen-bonding structure of water changes inside the active layer [6]. But the complex morphology of these classical membranes, along with their varied chemistry and their often proprietary synthesis methods, has made it difficult to better

understand the role of these fundamental processes or to further optimize them at the molecular scale.

2.2 Nanomaterials and clean water

Nanoporous materials have a great deal to offer over existing technology for desalination. In contrast with classical RO membranes, where water transports somewhat sluggishly via a solution-diffusion process [7], nanoporous membranes can allow for fast convective water flow across well-defined channels. Thanks to their small dimensions, nanopores can be used as filters on the basis of molecular size, since small molecules can pass through them while larger ones cannot. And because the dimensions of the nanopores are also comparable to the Debye screening length for electrostatic interactions and smaller than the mean free path between molecular collisions in water, the pores can also make use of other physical principles – such as charge or hydrophobicity – to reject ions or other molecular solutes.

The development of novel nanoporous membranes for desalination is a promising new field, yet it has received surprisingly little attention from materials scientists in recent years. Accordingly, some of the most basic questions about desalination across nanoporous membranes remain unanswered. What is known from published studies of nanoporous materials for clean water applications is primarily that (a) water across nanoscale channels can match and even outperform the flow predicted by continuum hydrodynamics; (b) adequately high salt rejection remains a challenge in most nanoporous membranes synthesized to date; (c) hydrophobic residues inside nanopores can contribute to flow by ordering the orientation of water molecules.

Until now, nanoporous membranes have been primarily examined for DNA sequencing [8] [9], virus removal [10], gas separation [11], [12], [13], and even voltage gating [14]. Early attempts to harness insights about fluid flow at the nanoscale gave rise to the field of nanofluidics, which has predominantly found applications in manipulation and sensing of DNA and other long-chain molecules and related topics. A comprehensive review of nanofluidics through 2005 is provided by Eijkel et al. [15].

But some of the most exciting results in this field came about when molecular dynamics studies began to suggest that water flow across CNTs could exhibit 'hyperlubricity' and give rise to flow rates much greater than predicted by the analogous macroscopic situation, Poiseuille flow across a cylindrical pipe **[16]**. Research by the Bakajin group at Lawrence Livermore National Laboratory made significant progress in replicating such flow patterns in the laboratory **[17]**, **[18]**, and attempts

were even made at synthesizing CNT membranes that could display extremely high water permeability while rejecting salt ions [19]. However, these membranes were fundamentally limited by their low salt rejection rates. Moreover, the difficulty of producing highly aligned and high-density – not to mention economically competitive – CNT arrays represents another important drawback of such membranes.

Several other classes of nanoporous materials have been explored for water desalination applications. Metal-organic frameworks (MOFs) can be designed to exhibit specific porous features at the nanometer-scale and have been explored for a number of membrane separation processes, including desalination. In particular, zeolites are aluminosilicate MOFs that can be coated onto ceramic membranes [20]. While zeolites and other MOFs have been regarded as a promising new approach to desalination technology, studies suggest that their relatively low water permeability may make them less attractive for desalination applications [21].

Rempe and colleagues at Sandia National Laboratories have taken an entirely different approach to nanoporous membranes. Their efforts have focused on biomimetic membranes that emulate the fundamental design principles of aquaporin channels in biological systems. They have found that aquaporin channels rely on a combination of narrow pore sizes to exclude solvated ions, hydrophobic residues to prevent water sticking, and C=O and NH dipoles to stabilize water molecules [22]. However, they have yet to build a synthetic membrane that can exhibit some of these bio-inspired principles.

2.3 Graphene as a nanoporous membrane

Because flux across a membrane scales inversely with the membrane's thickness, new types of ultrathin membranes offer the promise of greatly increased water permeability. Graphene, which consists of a 2D sheet of sp2-bonded carbon atoms in a hexagonal honeycomb lattice, is the ultimate thin membrane. Potential advantages of graphene over existing RO membranes include negligible thickness (one or several atomic layers) and high mechanical strength [23], which may enable faster water transport, low pressure requirements, and a wider range of operating conditions than previously possible. Nanopores can be introduced into graphene's structure, with the unsaturated carbon atoms at the pore edge passivated by chemical functional groups. Recently, experimental studies have explored a wide variety of methods for introducing nanopores in graphene, including focused ion beam exposure, diblock copolymer templating and chemical etching [24-27]. However, the potential applications of nanoporous graphene have thus far been limited to fields such as voltage gating and

gas separation [28]'[12], [13], [24-27]' [28-30], while the potential role of this material for water desalination remains largely unexplored.

In this thesis, I report computational results indicating that single-layer graphene can effectively separate salt from water for use in desalination systems. Using classical molecular dynamics simulations, I examined how the desalination dynamics change with pore size, pore chemistry and applied hydrostatic pressure. My calculations demonstrate that water can flow across a graphene membrane at rates in range of 10-100 L/cm^2/day/MPa, which is 2 to 3 orders of magnitude higher than diffusive RO membranes.

3 Computational methods

In order to characterize the behavior of NaCl salt water across a nanoporous graphene membrane, I have modeled a series of graphene nanopores with varying diameters and pore functionalizations. The pore sizes were varied from 1.5 to 55 Å^2, and I analyzed both pores passivated with commonly occurring hydroxyl groups (which are hydrophilic in nature) and hydrogen atoms (which are hydrophobic) in order to examine the effect of pore chemistry on desalination dynamics (see Figure 1). The choice of pore sizes was based on indications from previous studies. In particular, molecular dynamics studies by Suk et al. found that pure water can continue to flow across graphene pores down to 7.5 Å in diameter [31], and calculations by Sint et al. suggest that the chemical functionalization of graphene nanopores could be tuned to selectively reject certain solvated ions [32].

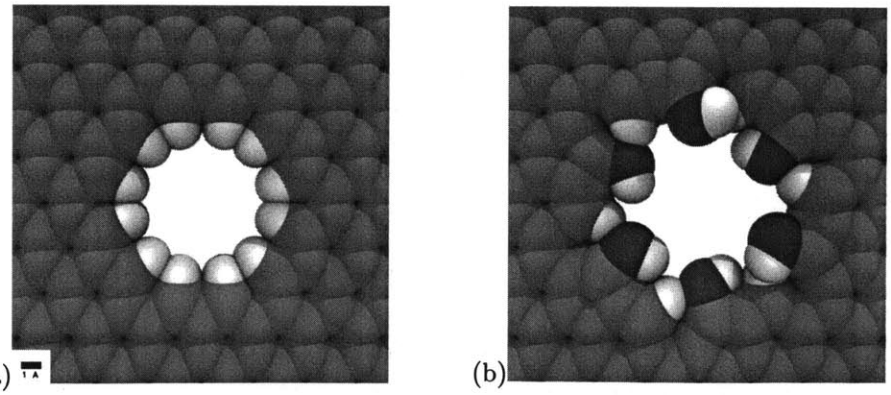

(a) (b)

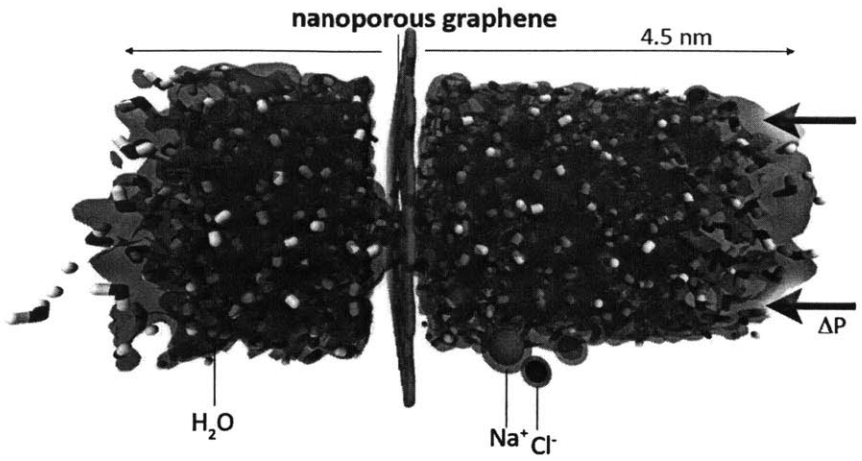

(c)

Figure 1: Hydrogenated (a) and hydroxylated (b) graphene pores, and (c) side view of the computational system investigated in this work.

Hydrogenated pores were obtained by passivating each carbon at the pore edge with a hydrogen atom. For hydroxylated pores, the unsaturated carbons along the pore edge were alternatively bonded with H- and OH- groups. Although this pore chemistry also contains hydrogen groups, these calculations indicate these pores are more thermodynamically stable with this alternating pattern because it prevents steric interactions between neighboring OH groups. Furthermore, the OH groups primarily govern the water-pore interactions because they extend further from the pore edge. In order to decouple the transport behavior of saltwater through the membrane from mechanical deformation phenomena, the carbon atoms in the membrane were held fixed during the simulations.

3.1 System Composition

Upon placing these different graphene systems in contact with a saltwater system consisting of 1,000 water molecules and 16 Na-Cl pairs, I applied pressures between 1 MPa and 1,500 MPa using a piston at the other end of the periodic simulation box. By tracking the number of water molecules on the permeate side of the membrane as a function of simulation time, I was able to determine the water permeability of the system (in units of volume of permeate per day, normalized per unit membrane area and applied pressure) and its output salinity, as well as a host of other dynamical properties as a function of time and spatial position.

The initial system consisted of a box measuring 75 Å in the z-direction and periodic x-y plane, with a unit cell cross-section of 30x30 Å. A two-dimensional, periodic sheet of porous pure graphene was modeled by starting with a perfect unit cell of 30x30 Å and

removing the carbon atoms contained within circles of varying diameters centered at the unit cell center. A layer of 113 water molecules was initially placed on the permeate side of the membrane in order to accurately model the flow dynamics.

The saltwater in the system contained 16 Na ions and 16 Cl ions solvated by 825 water molecules, corresponding to a salt concentration of 72 g/L [33]. A higher salinity than seawater (~35 g/L) was chosen in order to increase the occurrence of ion-pore interactions and obtain more precise results for a given system size and simulation time. Saltwater was generated using the Solvate and Ionize tools in the VMD software.

The graphene membrane was fixed at z = 60 Å, and a rigid piston was originally placed at z = 0 and subsequently allowed to push the water towards the membrane at a prescribed external pressure. After initially subjecting the system to pressures ranging from 1 MPa all the way to 1,500 MPa, I focused these calculations in the 100-200 MPa range in order to obtain well-converged statistics for the timescales involved in these MD calculations. Although these pressure values are significantly higher than what is typical for desalination (a few MPa), the fact that the timescales for flow scale linearly with applied pressure strongly suggests that these results will also hold valid at low pressures.

3.2 Parameters

Water was modeled using the TIP4P potential [34], while all other interactions were modeled using Lennard-Jones (LJ) and Coulombic terms. Na^+ and Cl^- ions and carbon-water interactions were modeled using the LJ parameters derived by Joung et al.[35] and Beu et al.[36] respectively. In simulations where hydroxyl groups were applied to the pore edges, the hydroxyl groups were described by the parameterization of phenol by Mooney. et al., which includes harmonic bond potentials for the C-O and O-H bonds, harmonic angles for the C-C-O and C-O-H angles, and harmonic dihedral potentials for the C-C-C-O and C-C-O-H dihedral angles, as well as Lennard-Jones (LJ) parameters for the interactions between each hydroxyl group and nearby atoms[37]. The initial conformation of the OH groups was obtained by performing a static energy minimization. Consistent with behavior of hydroxyl groups in phenol and related molecules, the O atoms preferentially sit in the plane of the graphene membrane, while the H atoms will place themselves in or out of plane depending on their electrostatic interactions with neighboring OH groups. A similar parameterization drawing from Muller-Plathe et al. was employed for hydrogen functional groups[38]. The parameters are summarized in Table 1.

The partial charges on membrane atoms were also held fixed during the calculations. Carbon atoms away from the pore edge were assigned neutral charge, while the partial charges on the functional groups and the neighboring carbon atoms were taken from the parameterization for the relevant functional group. Keeping partial charges fixed does not allow for electric charge rearrangement and polarization effects in the membrane, but the preferred electronegativities of the oxygen and hydrogen atoms passivating the pores ensure that the dominant Coulombic effects are captured accurately. The inter-atomic LJ parameters between species i and j were calculated using Lorentz-Berthelot mixing rules.

Table 1: LJ and charge parameters employed in this work

Element	C (sp2)	C_{COH}	H_{COH}	O_{COH}	C_{CH}	H_{CH}	H_w	O_w	Cl^-	Na^+
ϵ (kcal/mol)	0.0859	0.0703	0	0.155	0.046	0.0301	0	0.16275	0.0117	0.1684
σ (Å)	3.3997	3.55	0	3.07	2.985	2.42	0	3.16435	5.1645	2.2589
q (e)	0	0.2	0.44	-0.64	-0.115	0.115	0.5242	-1.0484	-1	1

3.3 Calculation details

All simulations were performed using the LAMMPS package [39]. The NVT ensemble was used with a Nosé-Hoover thermostat at 300 K with an initial Gaussian velocity distribution consistent with this temperature. After an equilibration time of 100 ps during which the external piston pressure was kept at P = 0, I carried out dynamic runs on the order of 5-10 nanoseconds with a timestep of 1 fs. The properties calculated below were obtained by averaging over 5 sets of initial conditions for each configuration to ensure that the quantities are converged.

3.4 Post-Processing

The resulting atomic trajectories were subsequently analyzed using the LAMMPS Pizza.py toolkit, as well as the H-Bonds, Radial Distribution Function and Volmap tools in VMD and in-house analysis scripts.

4 Results

4.1 Water permeability

The water flow across three different hydroxylated pores as a function of time is shown in Figure 2. The flow profiles show that the flow rate of water is constant in time and increases with pore diameter and applied pressure. For narrow enough pores, water

molecules are unable to pass, and no water permeation is observed during the entire trajectory. Conversely, when the water flow is fast enough, the curve eventually reaches a saturation point indicating that the entire reservoir of water molecules on the feed side has become depleted before the end of the simulation.

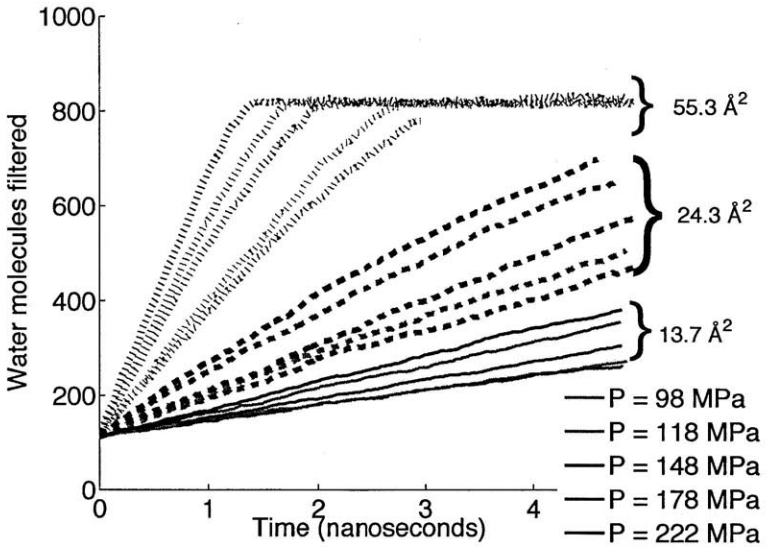

Figure 2: Water flow in hydroxylated pores as a function of simulation time. Flow rates, given by the slope of each curve, increase as a function of applied pressure as well as pore size. The largest pores allow water to flow at a constant rate that is proportional to applied pressure until the entire feed reservoir has become depleted.

Each trajectory begins with a linear regime in which water flows at a constant rate: the behavior of the system indicates that the effects of the finite size of the periodic simulation box – including the relative increase in feed salinity as water is gradually filtered through the membrane – are negligible in this regime. The slope of each flow curve in Figure 2 corresponds to the flow rate per unit of time, which was found to be proportional to applied pressure. Thus, we can extrapolate the dynamic quantities derived here down to the operating conditions more typical of reverse osmosis plants, ($\Delta P \approx 5$ MPa) by defining a water permeability normalized per unit of applied pressure. Assuming a relatively conservative membrane porosity of 10 percent, I have estimated the effective water permeability achieved in each system (see Figure 3). The water permeability, expressed in liters of output per cm^2 of membrane per day and per unit of applied pressure, ranges from zero (for the narrowest hydrogenated pore) to 129 $L/cm^2/day/MPa$ in the case of the largest hydroxylated pore simulated here. The permeability scales linearly with pore area, as expected from the Hagen-Poiseuille equation in classical fluid dynamics for flow across a cylindrical pore (see Figure 3)[40].

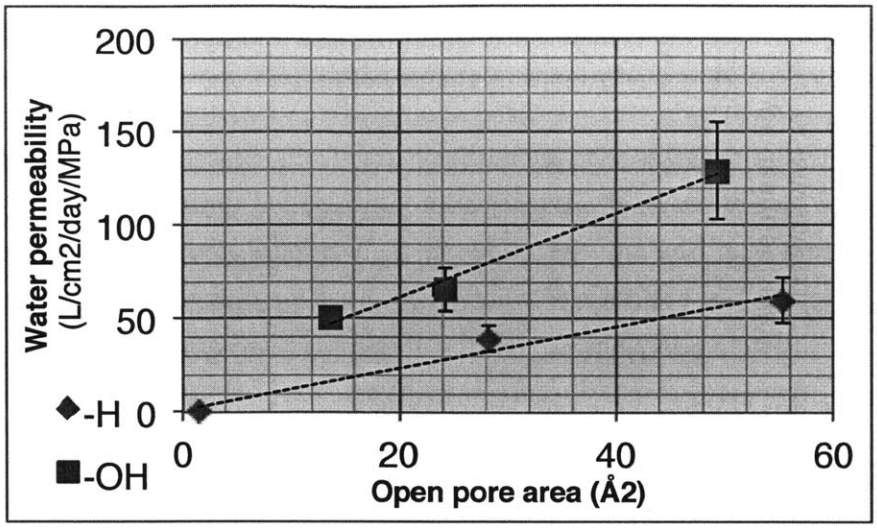

Figure 3: Computed water permeability for nanoporous graphene functionalized with hydrogen and hydroxyl groups for various pore sizes. Water permeability scales roughly linearly with the area of hydroxylated or hydrogenated pores.

On the other hand, the effect of pore chemistry has no clear analog in macroscopic fluid dynamics. For a given pore size, water permeability is significantly enhanced by hydroxylation: the permeability across the ~25 Å^2 pores (and the ~50 Å^2 pores) is larger by 69% (and 115%, respectively) compared with the hydrogenated case. This behavior is due to the fact that hydrophilic functional groups increase the water flux by allowing for a greater number of hydrogen-bonding configurations inside the pore.

4.2 Salt rejection

While pores must exceed a critical size in order to permeate water molecules, they must also be narrower than a maximum diameter in order to effectively hinder the passage of salt ions. The data for permeate salinity suggests that this maximum diameter is around 8 Å, i.e. that the majority of salt ions approaching the pore entrance are able to pass through the membrane beyond this diameter.

The calculated salt rejection for each nanoporous membrane is shown in Figure 4. Salt rejection is calculated from the salinity of the permeate solution at $t = t_{1/2}$ (defined as the time when half the water has flowed to the permeate side) relative to the initial salinity of the feed for the range of pore systems. For a perfectly rejecting membrane ($R = 100\%$), the permeate salinity is zero, while a membrane with no salt rejection ($R = 0\%$) would yield the same salinity in the permeate as in the initial feed. Figure 4 shows that salt rejection is close to 100% for the smallest hydrogenated and hydroxylated pore as well as for the medium hydrogenated pore. For the remaining

pores, the salt selectivity decreases both with pore size and applied pressure, reaching a minimum of 33% for the largest OH-functionalized pore at 222 MPa.

While salt rejection decrease with increasing pore size is expected from a size exclusion argument, the dependence of salt rejection on applied pressure is noteworthy. In particular, I find that the salt rejection of a given pore decreases at higher applied pressures, which is the opposite of what is observed in diffusive RO membranes[7]. I attribute this difference in behavior to the large effective volume of ions in solution, which causes them to respond more sensitively to pressure increases than water molecules. This is in contrast with the kinetics of ion passage across diffusive RO membranes, in which the governing driving force for salt passage is osmotic pressure and where water flux increases faster than salt flux with rising pressure.

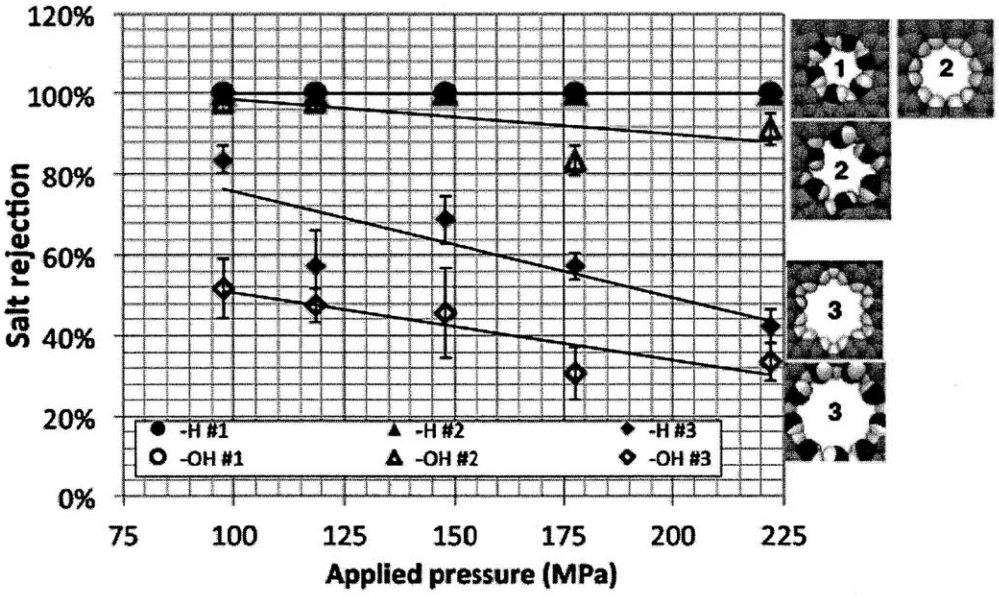

Figure 4: Average salt rejection as a function of pore type and pressure differential. The results indicate that smaller pores are capable of effectively rejecting salt, but that rejection performance decreases with higher pressures. Moreover, hydrogenated pores exhibit a stronger salt rejection performance than hydroxylated ones.

These results indicate that pore chemistry also has a notable effect on salt rejection. For a given pore size and applied pressure, the salt rejection is lower for hydroxylated pores. I attribute this effect to the fact that OH functional groups can hydrogen-bond with salt ions much like water molecules do, which results in a lower free energy barrier to ionic passage.

4.3 Water structure in the pore vicinity

The organization of water molecules in the vicinity of the pores plays a dominant role in both the water permeability and the salt rejection of a nanoporous graphene membrane. The water structure is in turn determined both by size effects (i.e. pore size) and chemical effects (i.e. pore functionalization). In order to further understand why hydroxylated pores exhibit higher water permeability and why hydrogenated pores are more effective at rejection salt, I have investigated several properties that indicate *how* water flows across each pore.

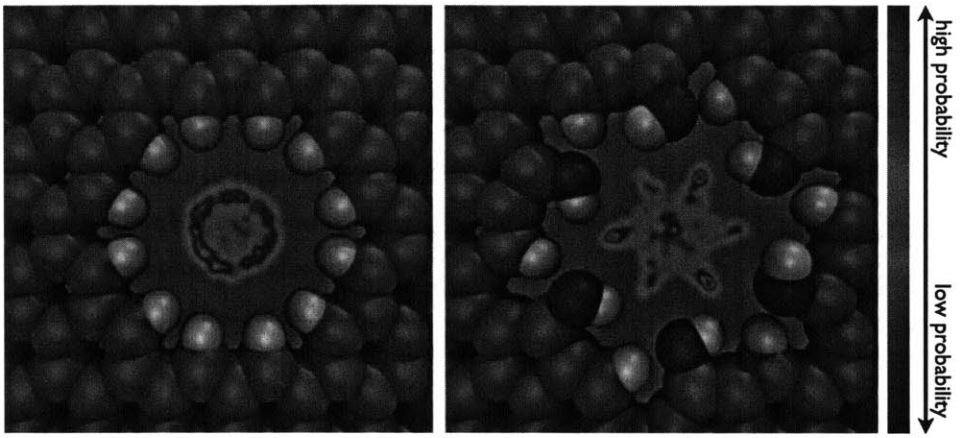

Figure 5: Oxygen density maps at inside a hydrogenated (left) and hydroxylated pore (right). Light blue indicates the region in which no water oxygens are found, while red regions indicate the highest probability of finding an oxygen atom.

In principle, the higher flow rates across hydroxylated pores could arise from either a broadening of the cross-sectional area available to water molecules, or from faster passage of each water molecule. To identify which effect is dominant here, I have calculated the density maps for oxygen atoms of water molecules inside H- and OH-functionalized pores (shown in Figure 5). Although the shapes of the density surfaces differ to reflect the radial and six-fold symmetry of the H- and OH-functionalized pore respectively, the figure reveals that the total cross-sectional area available for water passage across the H-functionalized pore is only smaller by about 25%. This decrease alone is insufficient to explain the 69-113% drop in water permeability found in hydrogenated pores, and therefore another factor must be at play.

I attribute this additional factor to an entropic effect. To illustrate this, the angular distribution function of water molecules in the vicinity of a graphene nanopore is plotted in Figure 6. The figure shows that water is more highly ordered in the vicinity of a hydrogenated pore. This higher level of ordering is consistent with the fact that

hydrogen passivation is hydrophobic and hence restricts the number of hydrogen-bonding configurations available to water molecules traversing the membrane. In contrast, OH- groups can hydrogen-bond with water and offer a smoother entropic landscape for water molecules to traverse, thus allowing for faster overall water flow. The effect of pore chemistry on water structure can thus explain why hydroxylated pores have higher water permeability than hydrogenated pores.

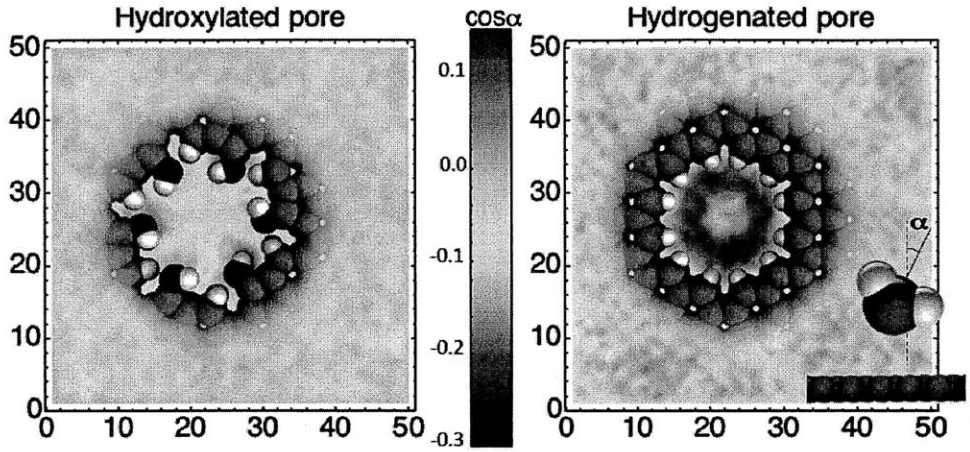

Figure 6: Angular distribution function (ADF) of water molecules with respect to the plane of the graphene membrane as a function of position. Red depicts increasingly positive values of $\boldsymbol{cos(\alpha)}$, indicating that the molecule's hydrogen atoms lie towards the membrane, while blue indicates negative values. The ADF is averaged over 5 Å on the feed side of the membrane for a hydroxylated pore (left) and hydrogenated pore (right) respectively.

4.4 Kinetic behavior

We can reproduce the qualitative behavior of water desalination across a nanoporous graphene membrane – including the entropic effect of pore chemistry and the salt rejection drop at higher pressures – with a simplified kinetic model involving a reduced number of variables. Assuming an Arrhenius model for both water and salt passage and neglecting finite size effects, we may approximate the rates of water and salt passage respectively as:

$$\dot{N}_w = A_0 e^{-\frac{\Omega_w P - (\Delta E + T\Delta S)}{kT}}$$

$$\dot{N}_s = B_0 e^{-\frac{\Omega_s P - (\Delta E + T\Delta S)}{kT}}$$

Here $A_0(T)$ and $B_0(T)$ represent the attempt rates for water and salt passage, respectively. These attempt rates may be treated as constant for a given pore size, chemistry, applied pressure, temperature and salt concentration. Ω_i denotes the effective volume of a molecule of species i: this effective volume multiplied by the applied pressure acts as a driving force for ion passage. The $(\Delta E + T\Delta S)$ terms represent the free energy barrier for species i associated with traversing the pore. For nanometer-scale pores, this free energy barrier is expected to be a large quantity, and the MD results described above indicate that it should be larger for a hydrophobic pore compared to a hydrophilic one since the entropic barrier for entering the pore is higher. In this kinetic model, the steady-state permeate salinity is given by the ratio of the two permeation rates:

$$\Sigma = \frac{\dot{N}_s}{\dot{N}_w}$$

The larger volume of solvated ions relative to water molecules can explain the observed salt rejection drop at higher pressures: although salt and water permeation rates both increase linearly with pressure, the salt has a larger effective volume. Accordingly, the salt flow rate increase is steeper than that of water and results in a lower overall salt rejection for increasing pressure. I take representative values for the effective volumes ($\Omega_w \sim 10^{-28}$ m^3, $\Omega_s \sim 10^{-27}$ m^3, $T = 300$) and the attempt rates expected from kinetic theory ($A_0 \sim 10^{11}$ s^{-1}, $B_0 \sim 10^{10}$ s^{-1}). To test this hypothesis that an entropic barrier can account for the contrasting properties of hydrophilic versus hydrophobic pores, I assign a larger value of ΔS to the hydrogenated pore than to the hydroxylated pore ($\Delta S =$ 4.5 k and 5.5 k respectively). For simplicity, I assume that the entropic barrier for salt passage is higher than for water passage by factor of 10 percent. The choice of an energy barrier ΔE is arbitrary since it does not appear in the expression for salt rejection. A further refinement to this model would be to specify two different values of ΔE for salt ions across OH- and H- functionalized pores, but the results below show that the present level of detail is enough to qualitatively reproduce the main observed trends.

The steady-state salt rejection predicted by this model is plotted in Figure 7. The plots indicate that the simple kinetic model proposed here qualitatively replicates the trends observed in the MD trajectories: (a) salt rejection is a decreasing function of applied pressure; (b) salt rejection is higher for a hydrogenated pore.

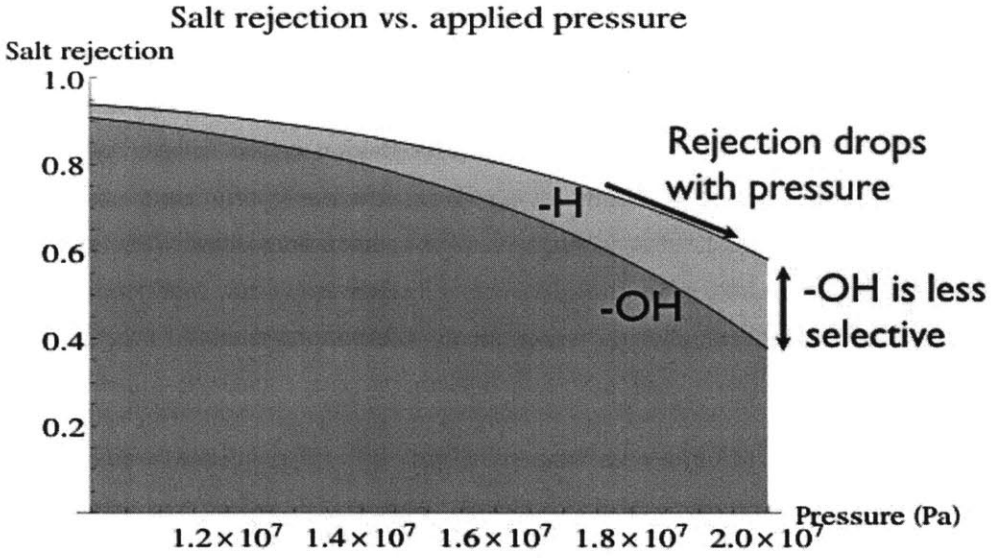

Figure 7: Predicted salt rejection across a hydrogenated (upper line) and hydroxylated (lower line) pore from a simple kinetic model. The model qualitatively replicates the observed decrease in salt rejection with increasing pressure, as well as the higher salt rejection performance of a hydrogenated pore. While this kinetic model neglects certain features of the MD system, including osmotic effects, finite size effects and collective phenomena, it qualitatively replicates the observed behavior. This lends support to the hypothesis that hydrophilic membrane chemistries enable faster flow rates by increasing the range of conformations and bonding configurations allowed inside the pore.

5 Discussion

Overall, the results described here indicate that graphene could act as a high-permeability desalination membrane. For illustrative purposes, the theoretical performance of the optimal graphene pore configurations examined here is plotted along with the experimental performance of RO in Figure 8. Among the pore configurations that exhibited both full salt rejection and water passage (28.3 $Å^2$ hydrogenated pore and 13.7 $Å^2$ hydroxylated pore), the water permeability ranged in the range of 39-66 L per cm^2·day·MPa. In contrast, experimentally observed permeabilities for RO barely exceed a few cl per cm^2·day·MPa (and values predicted from MD simulations lie in this range as well [41]).

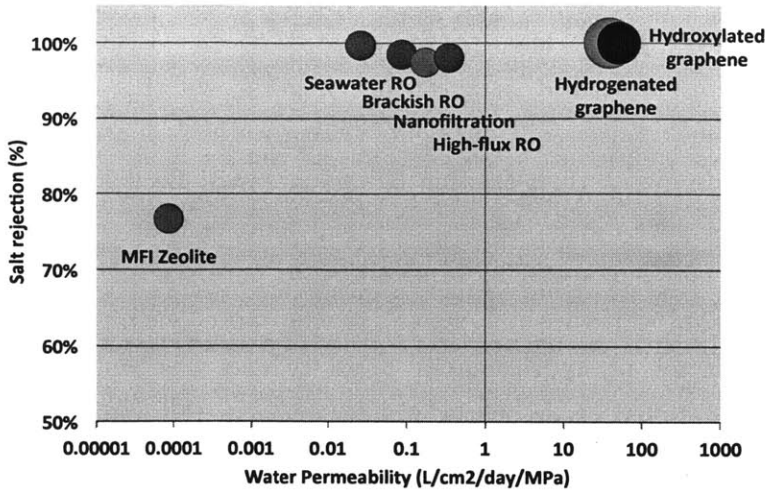

Figure 8: Performance chart for functionalized nanoporous graphene versus existing technologies. The graphene nanopores examined in this work could reject salt ions with a water permeability 2-3 orders of magnitude higher than commercial RO. The data for RO and MFI zeolites is adapted from Pendergast et al. [20].

In order to successfully design and build such a membrane, a couple of additional aspects should be taken into consideration. First is the challenge of achieving an extremely narrow pore size distribution in the membrane. Indeed, these calculations reveal that salt rejection performance is sensitive to pore size, meaning that a membrane contaminated with a few large pores might exhibit drastically lower salt selectivity. This highlights the importance of defect-free synthesis, which may be more readily achievable using self-assembly than with a beam drilling approach.

The second aspect is mechanical stability. While graphene is the strongest material known, the membrane envisioned in this work consists of a single atomic layer with a high porosity. While direct results for mechanical stability are outside the scope of the present work, previous computational work has found that graphene monolayers pinned every 40-160 Å could withstand pressures upwards of 500 MPa without ripping [42], with experimental results also confirming graphene's high robustness in bulge tests [11]. The fact that cross-flow configurations and spiral-wound membrane arrangements are often employed in desalination systems makes mechanical studies worthy of further exploration. The enhanced water permeability of nanoporous graphene could offer important advantages over existing RO technology. For a given water output, such a membrane would enable lower energy requirements thanks to lower operating pressures. It could also mean smaller and more modular desalination plants thanks to smaller membrane area requirements.

6 Conclusion

The MD simulations described in this work have shown that nanoporous graphene membranes are able to reject salt ions while letting water flow at permeabilities several orders of magnitude higher than existing RO membranes. By simulating saltwater flow across a variety of pore diameters and chemical functionalizations, I have established that desalination performance is most sensitive to pore size and pore chemistry. My examination of the structure of water in the pore vicinity revealed that the hydrophobic character of hydrogenated pores reduces the water flow by imposing additional conformational order on the system, even as the limited hydrogen bonding allows for greater salt rejection relative to hydroxylated pores.

This work highlights the promise of atomically thin, periodic nanostructures like graphene for water desalination. This approach strongly suggests that a bottom-up, systematic redesign of desalination membrane materials is possible and can yield significant improvements over existing technological methods. I expect that this work will add to the understanding of next-generation membranes for clean water technology.

7 Literature Sources

[1] M. A. Shannon, P. W. Bohn, M. Elimelech, J. G. Georgiadis, B. J. Mariñas, and A. M. Mayes, "Science and technology for water purification in the coming decades," *Nature*, vol. 452, no. 7185, pp. 301–310, Mar. 2008.

[2] UNESCO, "World Water Development Report 3: Water in a Changing World," UNESCO, Apr. 2010.

[3] M. Elimelech, "The global challenge for adequate and safe water," *Aqua-Journal of Water Supply: Research and ...*, 2006.

[4] Credit Suisse Research Institute, "Water: The pressure is rising," Credit Suisse Equity Research, Nov. 2009.

[5] L. Malaeb and G. M. Ayoub, "Reverse osmosis technology for water treatment: State of the art review," *Desalination*, pp. 1–8, Sep. 2010.

[6] W. A. P. Luck, "Structure of water and aqueous solutions," in *Synthetic Membrane Processes*, no. 2, G. Belfort, Ed. Troy, NY: Academic Press, 1984, p. 590.

[7] M. Williams, "A review of reverse osmosis theory," *EET Corporation and Williams Engineering Services Company, Inc*, 2003.

[8] G. Schneider, S. Kowalczyk, and V. Calado, "DNA translocation through graphene nanopores," *Nano Lett.*

[9] Z. S. Siwy and M. Davenport, "Nanopores: Graphene opens up to DNA," *Nature Nanotechnology*, vol. 5, no. 10, pp. 697–698, Oct. 2010.

[10] S. Yang, I. Ryu, H. Kim, J. Kim, S. Jang, and T. Russell, "Nanoporous membranes with ultrahigh selectivity and flux for the filtration of viruses," *Adv. Mater.*, vol. 18, no. 6, pp. 709–+, 2006.

[11] J. S. Bunch, S. S. Verbridge, J. S. Alden, A. M. van der Zande, J. M. Parpia, H. G. Craighead, and P. L. McEuen, "Impermeable atomic membranes from graphene sheets," *Nano Lett*, vol. 8, no. 8, pp. 2458–2462, 2008.

[12] D. Jiang and V. Cooper, "Porous Graphene as the Ultimate Membrane for Gas Separation," *Nano Lett*, 2009.

[13] S. Blankenburg, M. Bieri, R. Fasel, K. Muellen, C. A. Pignedoli, and D. Passerone, "Porous Graphene as an Atmospheric Nanofilter," *Small*, vol. 6, no. 20, pp. 2266–2271, 2010.

[14] S. N. Smirnov, I. V. Vlassiouk, and N. V. Lavrik, "Voltage-Gated Hydrophobic Nanopores," *ACS nano*, p. 110819092308063, Aug. 2011.

[15] J. C. T. Eijkel and A. V. D. Berg, "Nanofluidics: what is it and what can we expect from it?," *Microfluid Nanofluid*, vol. 1, no. 3, pp. 249–267, Apr. 2005.

[16] A. Alexiadis, "Molecular simulation of water in carbon nanotubes," *Chemical Reviews*, 2008.

[17] F. Fornasiero, J. B. In, S. Kim, H. G. Park, Y. Wang, C. P. Grigoropoulos, A. Noy, and O. Bakajin, "pH-Tunable Ion Selectivity in Carbon Nanotube Pores," *Langmuir*, vol. 26, no. 18, pp. 14848–14853, Sep. 2010.

[18] F. Fornasiero, H. G. Park, J. K. Holt, M. Stadermann, C. P. Grigoropoulos, A. Noy, and O. Bakajin, "Ion exclusion by sub-2-nm carbon nanotube pores," *P Natl Acad Sci Usa*, vol. 105, no. 45, pp. 17250–17255, 2008.

[19] B. Corry, "Designing carbon nanotube membranes for efficient water desalination," *J Phys Chem B*, vol. 112, no. 5, pp. 1427–1434, 2008.

[20] M. M. Pendergast and E. M. V. Hoek, "A review of water treatment membrane nanotechnologies," *Energy Environ. Sci.*, 2011.

[21] Z. Hu, Y. Chen, and J. Jiang, "Zeolitic imidazolate framework-8 as a reverse osmosis membrane for water desalination: Insight from molecular simulation," *J Chem Phys*, vol. 134, no. 13, p. 134705, 2011.

[22] S. Rempe, D. Rogers, Y. Jiang, S. Yang, P. Feibelman, and J. Merson, "Computational and experimental platform for understanding and optimizing water flux and salt rejection in nanoporous membranes.," *prod.sandia.gov*, 2010.

[23] Q. Lu and R. Huang, "Nonlinear Mechanics of Single-Atomic-Layer Graphene Sheets," *Int J Appl Mech*, vol. 1, no. 3, pp. 443–467, 2009.

[24] D. Wei, Y. Liu, Y. Wang, H. Zhang, L. Huang, and G. Yu, "Synthesis of N-Doped Graphene by Chemical Vapor Deposition and Its Electrical Properties," *Nano Lett*, vol. 9, no. 5, pp. 1752–1758, May 2009.

[25] M. Bieri, M. Treier, J. Cai, and K. Aït-Mansour, "Porous graphenes: two-dimensional polymer synthesis with atomic precision," *Chemical Communications*, 2009.

[26] M. Kim, N. S. Safron, E. Han, M. S. Arnold, and P. Gopalan, "Fabrication and Characterization of Large-Area, Semiconducting Nanoperforated Graphene Materials," *Nano Lett*, vol. 10, no. 4, pp. 1125–1131, Apr. 2010.

[27] S. Garaj, W. Hubbard, A. Reina, J. Kong, and D. Branton, "Graphene as a subnanometre trans-electrode membrane," *Nature*, 2010.

[28] H. Postma, "Rapid sequencing of individual DNA molecules in graphene nanogaps," *Nano Lett*, 2010.

[29] M. Hankel, Y. Jiao, A. Du, S. K. Gray, and S. C. Smith, "Asymmetrically Decorated, Doped Porous Graphene As an Effective Membrane for Hydrogen Isotope Separation," *J. Phys. Chem. C*, vol. 116, no. 11, pp. 6672–6676, Mar. 2012.

[30] A. W. Hauser and P. Schwerdtfeger, "Nanoporous Graphene Membranes for Efficient 3He/ 4He Separation," *The Journal of Physical Chemistry Letters*, vol. 3, no. 2, pp. 209–213, Jan. 2012.

[31] M. Suk and N. R. Aluru, "Water Transport through Ultrathin Graphene," *The Journal of Physical Chemistry Letters*, 2010.

[32] K. Sint, B. Wang, and P. Kral, "Selective ion passage through functionalized graphene nanopores," *J. Am. Chem. Soc.*, 2008.

[33] W. Humphrey and A. Dalke, "VMD: Visual molecular dynamics ," *Journal of molecular graphics*, 1996.

[34] W. L. Jorgensen, J. Chandrasekhar, J. D. Madura, R. Impey, M. L. Klein, and J. Chandrasekhar, "Comparison of Simple Potential Functions for Simulating Liquid Water," *J Chem Phys*, vol. 79, no. 2, pp. 926–935, 1983.

[35] I. Joung, "Determination of alkali and halide monovalent ion parameters for use in explicitly solvated biomolecular simulations," *The Journal of Physical Chemistry B*, 2008.

[36] T. Beu, "Molecular dynamics simulations of ion transport through carbon nanotubes. I. Influence of geometry, ion specificity, and many-body interactions," *J Chem Phys*, vol. 132, no. 16, p. 164513, 2010.

[37] D. Mooney, F. Mueller-Plathe, and K. Kremer, "Simulation studies for liquid phenol: properties evaluated and tested over a range of temperatures," *Chem Phys Lett*, vol. 294, no. 1, pp. 135–142, Sep. 1998.

[38] F. Müller-Plathe, "Local Structure and Dynamics in Solvent-Swollen Polymers," *Macromolecules*, vol. 29, no. 13, pp. 4782–4791, Jan. 1996.

[39] S. Plimpton, *LAMMPS-large-scale atomic/molecular massively parallel simulator*. Sandia National Laboratories, 2007.

[40] W. M. Deen, *Analysis of Transport Phenomena*. Oxford University Press, USA, 1998, p. 597.

[41] Y. Luo, E. Harder, R. S. Faibish, and B. Roux, "Computer simulations of water flux and salt permeability of the reverse osmosis FT-30 aromatic polyamide membrane," *J Membrane Sci*, vol. 384, no. 1, pp. 1–9, Nov. 2011.

[42] S. Jun, T. Tashi, and H. S. Park, "Size Dependence of the Nonlinear Elastic Softening of Nanoscale Graphene Monolayers under Plane-Strain Bulge Tests: A Molecular Dynamics Study," *Journal of Nanomaterials*, vol. 2011, pp. 1–6, 2011.